



# Process Sensitivity of GMAW: Aluminum vs. Steel

*Aluminum proves more sensitive to changes in current and wire-feed speed in comparison to steel*

BY T. P. QUINN

**ABSTRACT.** A heat-transfer model of the melting electrode in gas metal arc welding (GMAW) was used to compare the relative sensitivity of the process when welding with aluminum electrodes compared to that of steel electrodes. The aluminum model was verified with experiments for ER-1100 and ER-4043 electrodes. The dimensionless parameters in the model showed that conductive heat transfer dominates other effects in aluminum compared to steel, which causes the differences in sensitivity of the process to the input parameters (current, wire-feed speed, and/or voltage). If the steel and aluminum electrode extensions are compared at about the midpoint of the current range for electrodes of the same diameter (1.2 mm), the aluminum electrode is 28 times more sensitive to changes in the wire-feed speed than is the steel electrode. When welding with a 1.2-mm-diameter aluminum wire at 150 A, a 1% change in wire-feed speed causes an 8-mm change in the arc length. When welding with a 1.2-mm-diameter steel wire at 200 A, a 1% change in wire-feed speed causes a 0.5-mm change in the arc length. Similar sensitivity to changes in current is exhibited by aluminum. Dynamic analysis about the set points described above indicates the electrode extension in aluminum is many times more sensitive than steel to perturbations in wire-feed speed and current at low frequencies, but aluminum has a similar response to steel at high frequencies.

## Introduction

This paper uses a model of the melting electrode in gas metal arc welding (GMAW) of aluminum to explore the sensitivity of the process to changes in the

inputs: current, wire-feed speed (WFS), or voltage. The length of the electrode beyond the contact tube, the electrode extension, determines the arc length for a given contact tube-to-work distance (CTWD). The arc length controls the amount of heat input into the weld and, therefore, the geometry and quality of the finished weld in aluminum or steel GMAW (Ref. 1).

Many aspects make aluminum more difficult to GMA weld than low-carbon steel. When exposed to air, aluminum develops a "tenacious, refractory oxide film" that must be broken up before or during welding. Aluminum does not change color as it is heated to the welding temperature, making it more difficult to identify the pool. The steel welding electrode is stiffer and, in most cases, stronger than the aluminum electrode, making aluminum more difficult to feed properly (Refs. 2, 3). In addition, the research presented here shows the material properties of aluminum make the GMAW process substantially more sensitive to variations in the input parameters as compared to steel.

The need for lighter structures has renewed interest in increasing the amount of aluminum used, especially in transportation vehicles. The structures that are being considered for aluminum are

now made of steel and in many cases are joined using GMAW because of GMAW's high production rate. Hinrichs, et al. (Ref. 4), described the difficulty of using GMAW in the mass production of aluminum parts in an automated production line. They could achieve welding production rates comparable to those of steel, but found that aluminum welding systems did not meet the uptime requirements. Of particular concern in maintaining uptime are meltback events: the electrode melts all the way to the contact tube, and then the contact tube melts or the electrode fuses with the contact tube.

Little research has been devoted to explaining the differences between aluminum and steel GMAW. There have been a number of practical articles informing welders who are used to welding steel how to weld aluminum (Refs. 5-7). Excellent overviews of the GMAW process applied to aluminum were given by Saunders and Altshuler (Ref. 8) and Weymueller (Ref. 9).

The objective of the research presented here was to compare the physics of the aluminum GMAW process to the physics of the steel GMAW process. To do this, models of electrode extension in the aluminum GMAW process were developed and compared to previously developed models for steel.

## Model

The model was described in detail in Ref. 10 but will be briefly described here for clarity. The model solves the conduction equation for the heat transfer in the melting electrode — Fig. 1. It predicts the electrode extension  $l$  for a given material, current  $I$ , and WFS  $v$ . The arc length is the difference between the CTWD and  $l$ . Joule heat is generated in the electrode (Fig. 1), and heat is transferred to (and away) from the electrode at the boundaries. The melting end of the electrode is

## KEY WORDS

Aluminum GMAW  
Electrode Extension  
Arc Length  
Steel  
Aluminum  
Process Sensitivity

T. P. QUINN is with National Institute of Standards and Technology, Boulder, Colo.

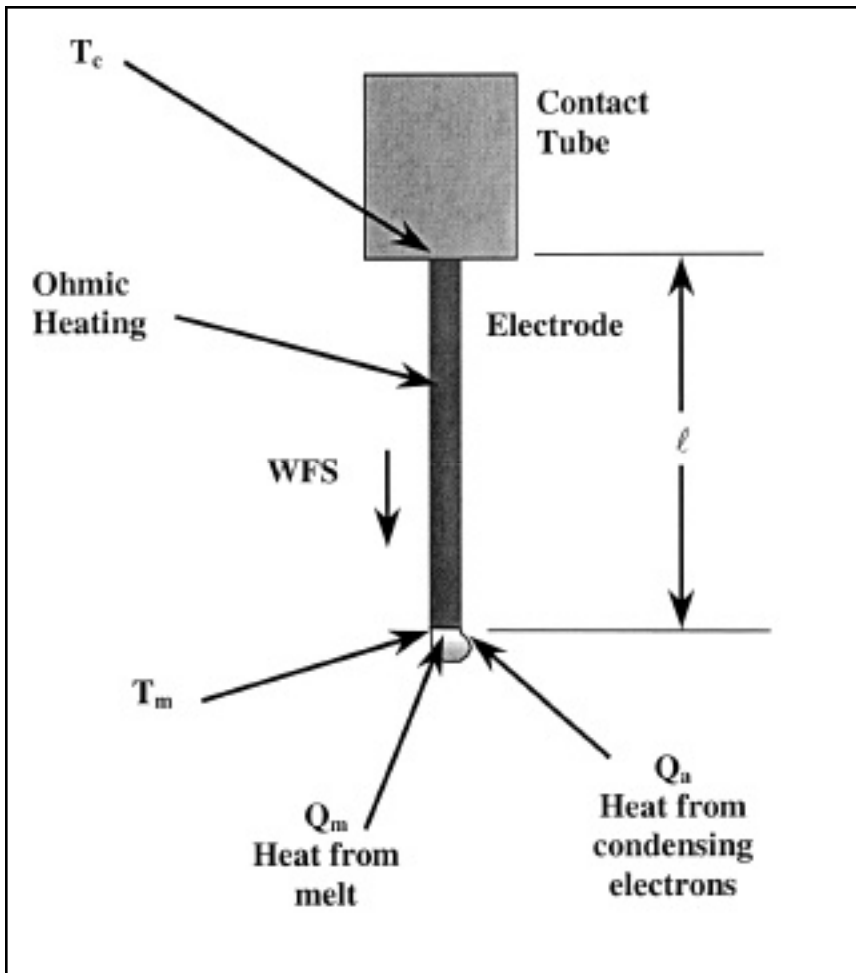


Fig. 1 — The heat sources in the model used to predict electrode extension.

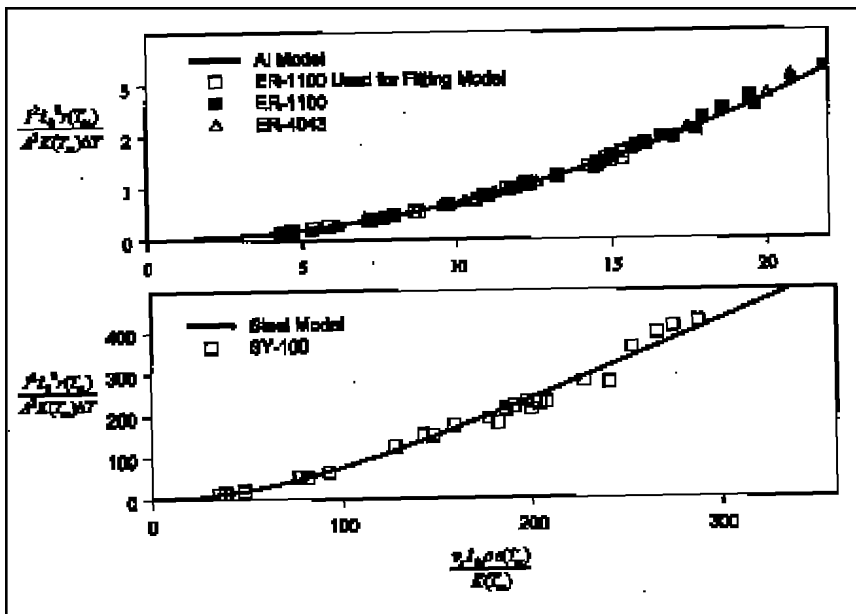


Fig. 2 — Comparison of experiments to model for aluminum and steel (Ref. 10).

modeled as having two sources of heat: the heat transferred by electrons condensing directly on the solid electrode  $Q_a$  and the heat transferred from the liquid melt  $Q_m$ . Following the analysis given in Ref. 10,  $Q_a$  and  $Q_m$  can be written as

$$Q_a = \gamma V_c I \tag{1}$$

$$Q_m = \frac{V_c (1 - \gamma) I}{2} \tag{2}$$

where  $V_c$  is the apparent condensation voltage and  $\gamma$  is the fraction of electrons condensing directly on the electrode.  $\gamma$  is unknown and must be found by fitting the model to experimental data. The governing equation is given as

$$\frac{1}{Z} K(T) \frac{T}{Z} + \frac{I^2 r(T)}{A^2} = v_z(t) \frac{T}{Z} + \frac{T}{t} c(T) \rho(T) \tag{3}$$

where  $A$  is cross-sectional area,  $t$  is time,  $T$  is temperature,  $K$  is thermal conductivity,  $c$  is the specific heat,  $r$  is the resistivity,  $Z$  is the spatial coordinate along the axis, and  $\rho$  is the density. The electrode is modeled as having a constant temperature  $T_c$  when it leaves the contact tube and is at the melting temperature at  $Z = l$ . The heat balance at the melting end allows  $l$  to be determined

$$-K(T) \frac{T}{Z} + \frac{Q_a(t)}{A} + \frac{Q_m(t)}{A} = \rho(T) L v_z(t) - \frac{dl}{dt} \tag{4}$$

where  $L$  is the latent heat.

The set of equations above was first solved for the steady-state response by setting the time derivatives equal to zero. The resulting ordinary differential equations were solved for  $T(Z)$  and  $l_0$ . (The 0 subscript will refer to the steady-state solution). To understand the dynamics of the process, the method of describing functions was used to develop frequency-response models about the steady-state set points. For details on the method of solution, see Ref. 10.

The thermophysical properties [ $K(T)$ ,  $c(T)$ , etc.] are allowed to vary with temperature in the model. However, there is little data throughout the pertinent temperature range for most alloys. Therefore, it was found and the model was verified on a nearly pure Al electrode (ER-1100); the property data are well known for the elements (Ref. 11). Later the model was used to predict the response of an aluminum alloy (ER-4043) using the pure Al property data. To find

the squared error between the experimentally determined  $I_0$  and the predicted  $I_0$  was minimized using a grid search technique (Ref. 10).

**Experiments**

Bead-on-plate welds were made with 1.19-mm ER-1100 and ER-4043 electrodes. A low-noise regulator was used as described in Ref. 12 to maintain constant current. To obtain measurements of  $I_0$ , a 10-mW He-Ne laser and 632-nm band-pass filter were used to create a shadowgraph of the electrode and base plate (Ref. 13). The shadowgraph images were recorded with a high-speed video system. The contact tube, the electrode, and the workpiece were imaged. The images were processed digitally to extract  $I_0$  and CTWD.

The current was measured with a Hall-effect transducer with an absolute error of 1%. The voltage between the torch and the baseplate was measured within 0.5% absolute error. The wire-feed speed  $v_z$  was measured as the electrode entered the wire feeder. A pinch roller (16 mm diameter) was attached to an optical encoder (5000 pulses/rev.) and the resulting pulse train was frequency converted to give a voltage signal proportional to  $v_z$ . The rms uncertainty from calibration tests for the transducer was 2 mm/s. The CTWD was set at 17 mm.

Two series of ER-1100 was collected. The model was fit to the data from the first series of tests and verified using data from the second series.

**Results and Discussion**

**Steady-State Results**

The fraction of electrons condensing directly on the electrode was found to be 0.035 by fitting the model to the first series of the data for the aluminum ER-1100 electrode — Fig. 2. This compares to 0.08 found with the steel electrode (Ref. 10). The model was solved in dimensionless form; therefore, the model actually predicts the dimensionless group

$$q = \frac{I^2 l_0^2 r(T_m)}{A^2 K(T_m) T}$$

if given the dimensionless group

$$W = \frac{v_z l_0 \rho c(T_m)}{K(T_m)} \quad (\text{Peclet number}).$$

$T$  is the temperature difference between the melting point and room temperature.  $T_m$  is the temperature at the melting point. To compare the model to the experiments, the rms difference between the

**Table 1 — The Dependence of Electrode Extension on Current for a Given Wire-Feed Speed**

Electrode	Case	Wire-Feed Speed (mm/s)	Electrode Extension Range (mm)	Change in Electrode Extension (mm)	Current Range (A)	Change in Current (A)	Slope (mm/A)
Aluminum 1.2 mm dia.	All	80 (189 in./min)	7-15	8	123.1-124.1	1.03	-7.83
	A12	100 (236 in./min)	7-15	8	153.3-154.9	1.59	-5.02
	A13	120 (283 in./min)	7-15	8	183.2-185.5	2.29	-3.49
Steel E100S-1 1.2 mm dia.	St1	100 (236 in./min)	7-15	8	197.8-225.9	28.10	-0.28
	St2	125 (295 in./min)	7-15	8	232.3-274.7	42.44	-0.19
	St3	150 (354 in./min)	7-15	8	262.8-320.3	57.46	-0.14

**Table 2 — The Dependence of Electrode Extension on Wire-Feed Speed for a Given Current**

Electrode	Case	Current (A)	Electrode Extension Range (mm)	Change in Electrode Extension (mm)	Wire-Feed Speed Range (mm/s)	Change in Wire-Feed Speed (mm/s)	Slope $\frac{\text{mm}}{\text{mm/s}}$
Aluminum 1.2 mm dia.	A14	100	7-15	8	64.4-64.8	0.4	18.3
	A15	150	7-15	8	96.8-97.8	1.0	8.1
	A16	200	7-15	8	129.5-131.3	1.8	4.5
Steel E100S-1 1.2 mm dia.	St4	200	7-15	8	88.0-101.5	13.5	0.57
	St5	250	7-15	8	111.9-139.2	27.2	0.29
	St6	300	7-15	8	138.7-184.2	45.5	0.17

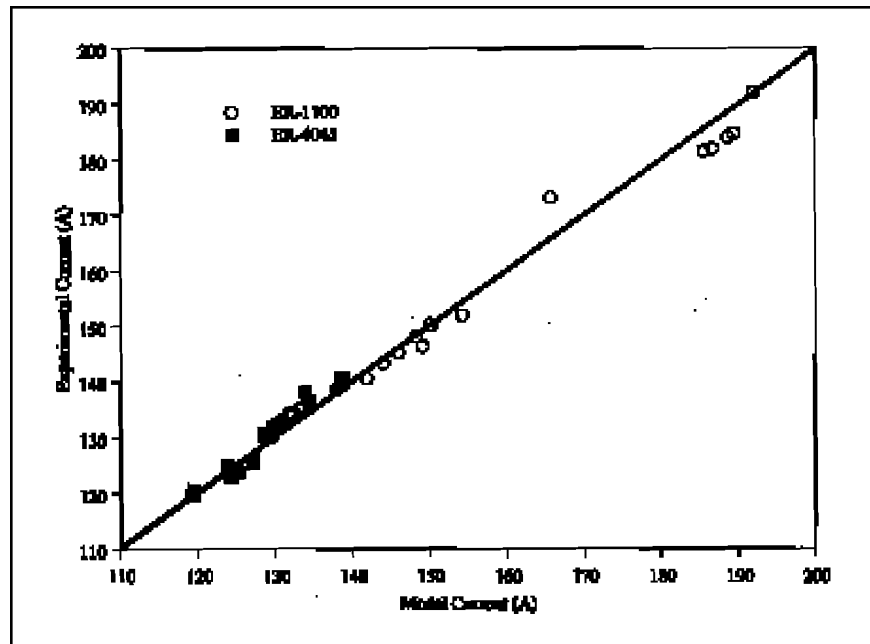


Fig. 3 — Experiment vs. model predicted current for the aluminum electrodes. The rms difference between the model and the experiment is 3 A for the ER-1100 electrode and 2 A for the ER-4043 electrode.

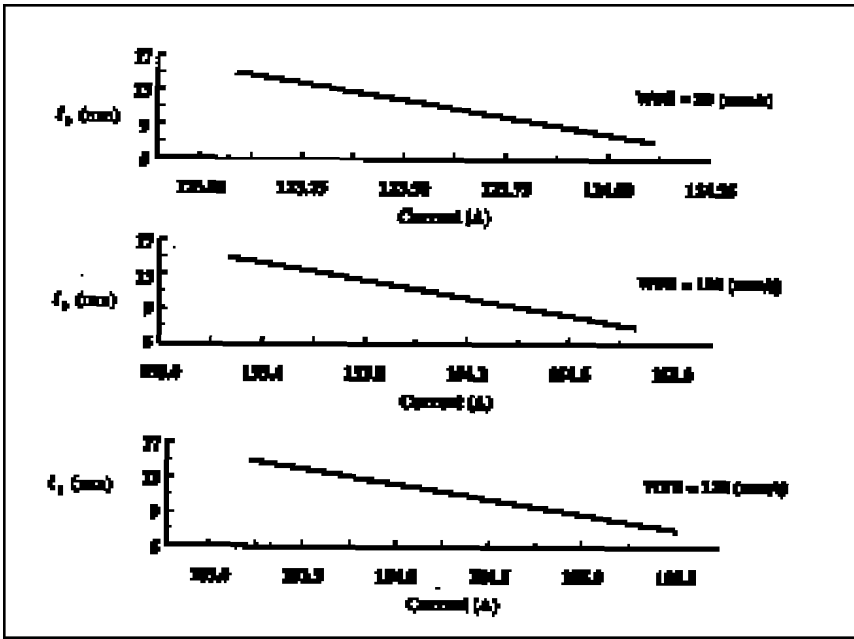


Fig. 4 — Dependence of the electrode extension on current for the aluminum electrodes.

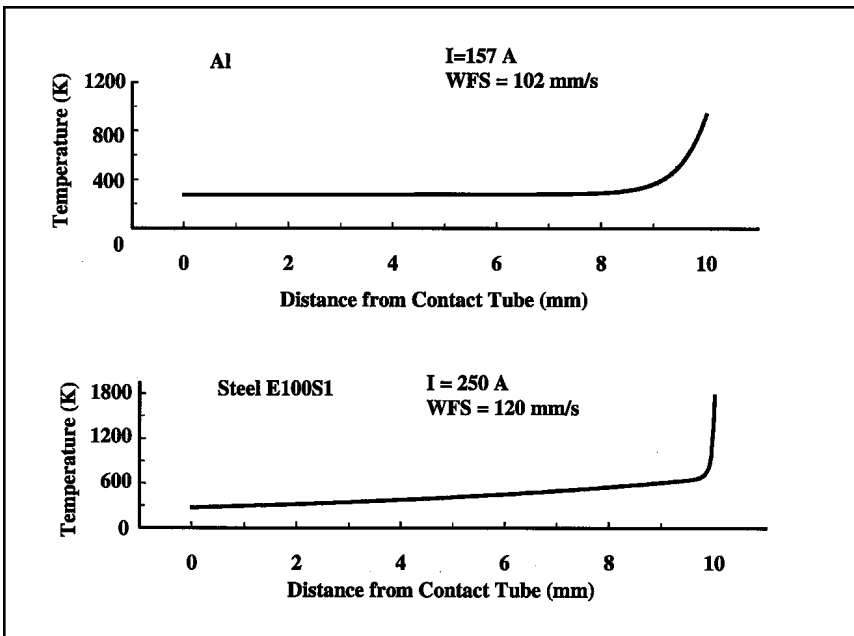


Fig. 5 — The predicted temperature distributions for E1100 and E100S-1 electrodes. The welding conditions are taken from about the middle of the practical welding range for a 17-mm CTWD.

model and experimental results was first computed; it was then normalized by the largest experimental  $q$  for the ER-1100 electrode ( $q = 3.3$ ). The rms difference between the model  $q$  and the experimental  $q$  is 1% for the ER-1100 data used to find  $\psi$ , 2% for the remaining ER-1100 data, and 2% for the ER-4043 electrode.

The Peclet number  $W$  is the ratio of the amount of energy convected by the movement of the electrode to the energy transferred by thermal conduction (Ref. 14). From the figure, the Peclet number is about an order of magnitude higher for the steel electrode because thermal conduction is more important in the alu-

minum wire due to its higher thermal conductivity. The other dimensionless group  $q$  is the ratio of the Joule heating to the heat transferred by conduction. Because of the lower electrical resistivity and the higher thermal conductivity of aluminum, this dimensionless group is about two orders of magnitude higher for steel than for the aluminum even though the melting point of steel is higher than that of aluminum (~1800 K for steel vs. 932 K for Al). Again, thermal conduction is more important than resistive heating in aluminum relative to steel.

Two other dimensionless groups that are applicable to this problem concern the physics that occurs at the melting boundary of the electrode. Making Equation 4 dimensionless creates the groups

$$\psi = \frac{\rho L v_z}{K(T_m) T} \text{ and } \chi = \frac{V I_0}{AK(T_m) T}$$

is the ratio of the amount of energy needed to change the phase of the metal from solid to liquid at the boundary to the amount of energy carried away by conduction at the boundary.  $\chi$  is the ratio of the energy deposited at the boundary by the condensing electrons to the amount conducted away. For the aluminum electrodes tested,  $\psi$  ranges from about 2 to 10; for the steel electrode,  $\psi$  ranges from about 10 to 70. Thus, at the boundary, thermal conduction is more dominant in aluminum than steel. For the aluminum electrodes tested,  $\chi$  ranges from about 7 to 40; for the steel electrode,  $\chi$  ranges from about 40 to 250. Again, the higher conductivity of aluminum and its lower melting temperature control the physics at the boundary.

The dimensionless groups have three parameters the operator chooses for a given electrode ( $K, A, T, r, \rho, c$  given): the current  $I$ , the WFS  $v_z$ , and the electrode extension (or really the arc length,  $CTWD - l_0$ ). When using a constant-voltage power source, the wire-feed speed and the voltage are commonly used to control the process. The arc length is about proportional to the voltage (Ref. 1), so in this case the arc length and wire-feed speed are selected. With the curves in Fig. 2, the model can be used to predict any one of the three process variables, given the other two — Fig. 3.

The steady-state model can be used to illustrate some fundamental differences between aluminum and steel. If the wire-feed speed is held constant and the current varies by a small amount, the current is proportional to the electrode extension for both the aluminum and the steel electrode to a correlation factor of over 0.999 — Fig. 4. In Table 1, results are presented

for wire-feed speeds that cover the range of practical welding conditions (Ref. 9) for both the steel and the aluminum electrodes at 1.2 mm diameter. When using the slope of the line that relates current to electrode extension for comparison, the aluminum electrode is at least an order of magnitude more sensitive to variations in current than is the steel electrode. At the low end of the welding range in aluminum, a 1-A variation in the current (about 0.8%) can change the electrode extension by 8 mm (0.315 in.). For the 17-mm CTWD used in the aluminum experiments, the 1-A change for the WFS of 80 mm/s would change the arc length from 10 to 2 mm.

A similar analysis using the steady-state model can be used to understand the differences between sensitivity of arc length to changes in wire-feed speed. Here the current will be held constant and the wire-feed speed varied. Again, the aluminum electrode is at least an order of magnitude more sensitive to changes in wire-feed speed than the steel electrode (Table 2, slope). At the lowest practical current for this electrode (100 A), a 0.6% change in the wire-feed speed causes an 8-mm change in the electrode extension. A 1% change in the wire-feed speed would cause a 69% change in the arc length (for a CTWD of 17 mm). The steel electrode is less sensitive: a 1% change in the wire-feed speed at 200 A causes a change in the arc length of just 0.5 mm or 3% of a 17-mm CTWD.

The steady-state model can be used to predict the temperature distribution and the voltage drop along the electrode. The steel electrode's temperature climbs linearly from the contact tube with a rapid increase near the end of the electrode because of the heat added to the end from the condensing electrons and the melt — Fig. 5. Conduction is more important in the aluminum electrode, which causes a slower increase in the temperature. The total potential drop in the electrode can be found by integrating the temperature-dependent electrical resistivity along the electrode. For the cases presented in Fig. 5, the drop in the aluminum electrode is 0.03 V, and the drop in the steel electrode is 0.3 V. The one order-of-magnitude difference is due to the higher melting temperature of steel and its higher electrical resistivity. For the aluminum electrode in Fig. 5, with a CTWD of 17 mm, the total voltage fall from the contact tube to the baseplate is about 20 V. The drop in the electrode is just 0.2% of the total.

**Dynamic Results**

The model predicts that the aluminum electrode exhibits a characteristic

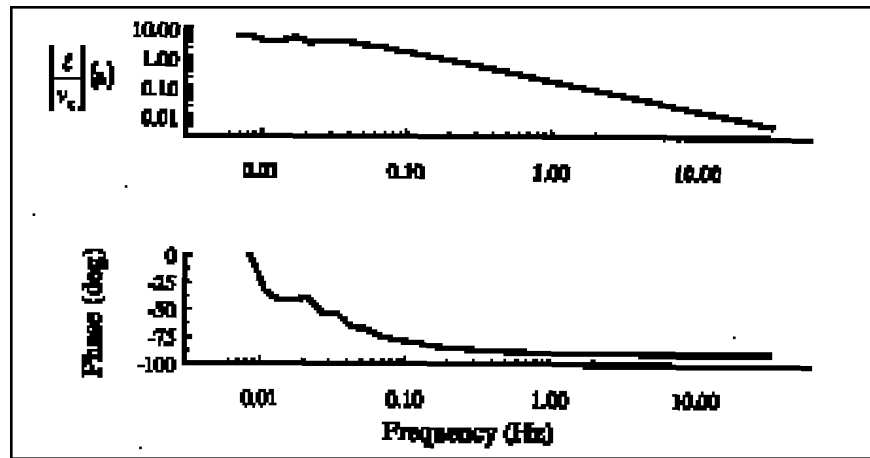


Fig. 6 — Modeled frequency response of the aluminum electrode to perturbations in wire-feed speed. The current is 157 A, the mean wire feed speed is 102 mm/s, and the mean electrode extension is 10 mm.

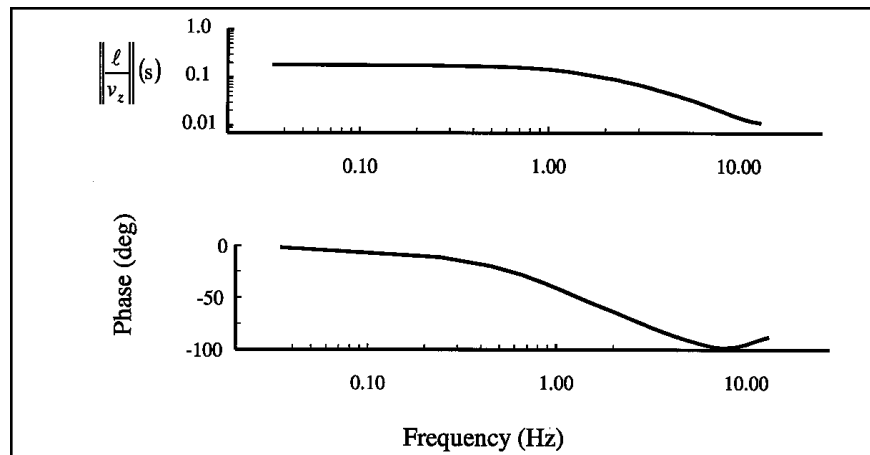


Fig. 7 — Modeled frequency response of the steel electrode to perturbations in wire-feed speed. The current is 250 A, the mean wire-feed speed is 120 mm/s, and the mean electrode extension is 10 mm.

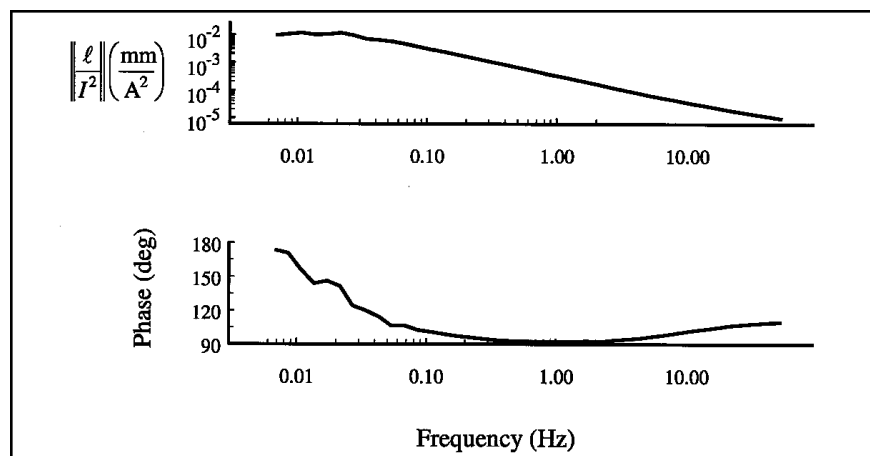


Fig. 8 — Modeled frequency response of the aluminum electrode to perturbations in the squared current. The mean current is 157 A, the wire-feed speed is 102 mm/s, and the mean electrode extension is 10 mm.

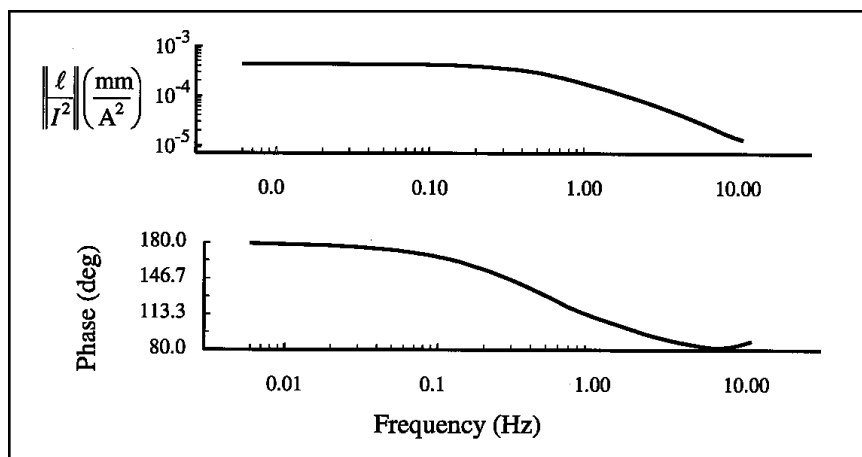


Fig. 9 — Modeled frequency response of the steel electrode to perturbations in squared current. The mean current is 250 A, the wire-feed speed is 120 mm/s, and the mean electrode extension is 10 mm.

frequency response similar to that of steel. The response of a steel electrode is detailed in Ref. 10, but also in a much earlier work of Manz (Ref. 15). The electrode extension (or arc length for constant CTWD) responds to perturbations in wire-feed speed or current like a first-order filter — Figs. 6 and 7. The frequency where the magnitude of the response begins to roll off is often called the cut-off frequency. The cut-off frequency is lower for aluminum than for steel. When the WFS is perturbed, the cut-off frequency for the aluminum electrode is about 0.03 Hz when welded near the middle of its current range — Fig. 6. The cut-off frequency for the steel electrode is about 1.01 Hz welded near the middle of its current range — Fig. 7. When comparing these two cases, the aluminum electrode is still more sensitive to perturbations in WFS until about 10 Hz, even though its cut-off frequency is 3% that of the steel electrode. Aluminum is about 100 times more sensitive at low frequencies

Similar comparisons can be made between aluminum and steel for perturbations in current. The cut-off frequency is lower for aluminum than for steel. When the current squared is perturbed, the cut-off frequency for the aluminum electrode is approximately 0.05 Hz, when welded near the middle of its current range — Fig. 8. The cut-off frequency for the steel electrode is about 0.66 Hz when welded near the middle of its current range — Fig. 9. When comparing these two cases, the aluminum electrode is still more sensitive to perturbations in current squared at least until 60 Hz, even though its cutoff frequency is 8% that of the steel electrode. Aluminum is approximately 33 times more sensitive at low frequencies (< 0.02 Hz).

## Conclusions

1) Aluminum GMAW is inherently much more sensitive to changes in the set point (current, wire-feed speed, and/or voltage) than for steel. For similar conditions at the center of the practical current ranges (Cases Al5 and St5, Table 2), the aluminum electrode extension is 28 times more sensitive to changes in the WFS set point than steel. For similar conditions at the center of the practical current ranges (Cases Al2 and St2, Table 1), the aluminum electrode extension is 26 times more sensitive to changes in the current set point than steel.

2) The physical reason for the increased sensitivity to changes in the process variables of aluminum compared to steel are the higher thermal conductivity, lower electrical resistivity, and lower melting point of aluminum. The controlling dimensionless groups for aluminum are from one to two orders of magnitude different from those of steel. Conductive heat transfer is more important in aluminum. In steel, resistive heating, phase change, and convection are relatively more important.

3) If the WFS (or current) is perturbed around a given set point, the GMAW process acts as a first-order filter in electrode extension for both steel and aluminum. For perturbations in WFS, the aluminum has a lower cut-off frequency than does steel (0.03 vs. 1.01 Hz), but has a much higher sensitivity to low frequencies (100 x) (again comparing at the center of the range for currents). Similar comparisons can be made for perturbations in current.

4) Because of the lower resistivity of aluminum, the voltage drop across the electrode extension in the aluminum is smaller by an order of magnitude than

that in steel. Using the same comparison as in conclusion 3, the voltage drop in aluminum is 0.03 V, and the drop in the steel electrode is 0.3 V.

5) ER 4043 can be modeled using the same thermophysical properties as those for a nearly pure aluminum electrode (ER 1100).

## References

1. Madigan, R. B., Quinn, T. P., and Siewert, T. A. 1995. Control of gas-metal-arc welding using arc-light sensing. Gaithersburg, Md., National Institute of Standards and Technology, Report No. NISTIR 5037, p. 9.
2. Oates, W. R., ed. 1996. Welding Handbook. Eighth edition, Vol. 3, American Welding Society, Miami, Fla.
3. Cary, H. B. 1998. Modern Welding Technology. Fourth edition, Prentice Hall, Upper Saddle River, N.J.
4. Hinrichs, J. F., Noruk, J. S., McDonald, W. M., and Heideman, R. J. 1995. Challenges of welding aluminum alloys for automotive structures. *Svetsaren* 50 (3): 7–9.
5. Ryan, P. 1988. Tips on welding aluminum with the GMAW process. *Welding Journal* 67(12): 43–45.
6. Cary, H. B. 1998. Welding aluminum. *World of Welding* 11:14–16.
7. Altshuller, B., and Bower, D. 1999. How to change from steel to aluminum. *The Fabricator* 29(11): 36–38.
8. Saunders, H. L., and Altshuller, B. 1986. The GMAW process applied to aluminum. *Proc. The Aluminum Joining Seminar*, p. 16.
9. Weymueller, C. R. 1981. Aluminum welding — an engineering guide. *Welding Design and Fabrication* 54 (5).
10. Quinn, T. P., Madigan, R. B., and Siewert, T. A. 1994. An electrode extension model for gas metal arc welding. *Welding Journal* 73(10): 241-s to 248-s.
11. Touloukian, Y. S., ed. 1967. The Elements. Vol. 1, Thermophysical properties of high temperature solid materials. New York: MacMillan Co.
12. Heald, P. R., Madigan, R. B., Siewert, T. A., and Liu, S. 1991. Droplet transfer modes for a MIL 100S-1 GMAW electrode. Gaithersburg, Md., NIST, Report No. NISTIR 3976.
13. Allemand, C. D., Schoeder, R., Ries, D. E., and Eagar, T. W. 1985. A method of filming metal transfer in welding arcs. *Welding Journal* 64(1): 45–47.
14. Krieth, F., and Black, W. Z. 1980. Basic Heat Transfer. Cambridge: Harper and Row.
15. Manz, A. F. 1968. Effect of periodic variation of system parameters on the arc-power supply system. *Transactions on Industry and General Applications of IEEE* 4(2): 207–213.